

## Role of Helix 0 of the N-BAR Domain in Membrane Curvature Generation

Fábio Fernandes,\* Luís M. S. Loura,<sup>†‡</sup> Francisco J. Chichón,<sup>§</sup> Jose L. Carrascosa,<sup>§</sup>  
Alexander Fedorov,\* and Manuel Prieto\*

\*Centro de Química-Física Molecular, Instituto Superior Técnico, Lisbon, Portugal; <sup>†</sup>Centro de Química de Évora, Évora, Portugal;  
<sup>‡</sup>Faculdade de Farmácia, Universidade de Coimbra, Coimbra, Portugal; and <sup>§</sup>Centro Nacional de Biotecnología-Consejo Superior de Investigaciones Científicas, Madrid, Spain

**ABSTRACT** A group of proteins with cell membrane remodeling properties is also able to change dramatically the morphology of liposomes *in vitro*, frequently inducing tubulation. For a number of these proteins, the mechanism by which this effect is exerted has been proposed to be the embedding of amphipathic helices into the lipid bilayer. For proteins presenting BAR domains, removal of an N-terminal amphipathic  $\alpha$ -helix (H0-NBAR) results in much lower membrane tubulation efficiency, pointing to a fundamental role of this protein segment. Here, we studied the interaction of a peptide corresponding to H0-NBAR with model lipid membranes. H0-NBAR bound avidly to anionic liposomes but partitioned weakly to zwitterionic bilayers, suggesting an essentially electrostatic interaction with the lipid bilayer. Interestingly, it is shown that after membrane incorporation, the peptide oligomerizes as an antiparallel dimer, suggesting a potential role of H0-NBAR in the mediation of BAR domain oligomerization. Through monitoring the effect of H0-NBAR on liposome shape by cryoelectron microscopy, it is clear that membrane morphology is not radically changed. We conclude that H0-NBAR alone is not able to induce vesicle curvature, and its function must be related to the promotion of the scaffold effect provided by the concave surface of the BAR domain.

### INTRODUCTION

Control of membrane remodeling is essential in clathrin-mediated endocytosis (CME) as different types and levels of curvature are required at each stage of the budding of clathrin-coated vesicles (1,2). Several of the proteins thought to play relevant roles in CME (dynamin, amphiphysin, endophilin, and epsin) were recently shown to induce tubulation in protein-free spherical liposomes, indicating a potential role as mediators in the membrane remodeling observed during CME (3–6).

The BAR (Bin, amphiphysin, Rvs) domain, found in amphiphysin, endophilins, and a wide variety of other proteins with or without known function in CME (7), is able to bind lipid membranes, generate tubulation (both *in vivo* and *in vitro*) and to sense bilayer curvature (5,8). This versatile domain has a banana shape and dimerizes in membranes, giving rise to a positively charged concave surface that binds to lipid bilayers. This concave surface is likely to be the reason why the domain presents higher affinities for high curvature liposomes *in vitro*.

Several BAR domains also present an N-terminal sequence that forms an amphipathic helix upon membrane binding (9). This sequence is here referred to as helix 0 (H0-NBAR). BAR domains presenting this sequence are called N-BAR and are able to bind to liposomes and induce tubulation with much higher efficiency, even though sensitivity for curvature is lost (8). After a point mutation in H0-NBAR of a

conserved hydrophobic residue (F) to an acidic residue (E), lipid binding and tubulation were abolished for endophilin (5), and reduced for the corresponding mutation in amphiphysin1 (8). Conservative mutations of the same residue (F to W) had no effect (5). These results point to an important role of H0-NBAR in membrane remodeling by N-BAR domains, and this role is likely to be dependent on membrane embedding of H0-NBAR. The exact function of H0-NBAR in membrane tubulation is, however, still elusive.

The H0 fragment from BRAP (breast-cancer-associated protein)/Bin2, one of the first BAR domains containing proteins to be identified (10,11), presents great homology to other N-terminal amphipathic fragments of BAR domain-containing proteins (Fig. 1). The N-BAR domain of BRAP was already shown to tubulate liposomes in an identical fashion to other N-BAR domains. The mutations performed on the N-BAR domain from BRAP had also analogous effects in lipid tubulation as the corresponding mutants of the N-BAR domain of amphiphysin, corroborating that the same liposome tubulation mechanism was shared by the two proteins. Here we investigated the interaction of a peptide comprising the H0-NBAR fragment of BRAP with model lipid membranes. We performed a thorough study of the effects of partition of the N-BAR N-terminal domain to lipid membranes on both structure and dynamics of H0-NBAR itself and the interacting lipid membranes. We show that the N-terminal fragment of the N-BAR domain assumes in effect an  $\alpha$ -helical structure upon membrane binding, and that membrane binding is dependent on the presence of anionic phospholipids but is virtually insensitive to both anionic lipid structure and liposome curvature. Through FRET (Förster resonance energy transfer), it is demonstrated that H0-NBAR

Submitted May 21, 2007, and accepted for publication November 26, 2007.

Address reprint requests to Manuel Prieto, Centro de Química-Física Molecular, Complexo I, Instituto Superior Técnico, Av. Rovisco Pais, 1049-001 Lisbon, Portugal. Tel.: 35-121-841-9219; Fax: 35-121-846-4455; E-mail: manuel.prieto@ist.utl.pt

Editor: Antoinette Killian.

© 2008 by the Biophysical Society  
0006-3495/08/04/3065/09 \$2.00

doi: 10.1529/biophysj.107.113118

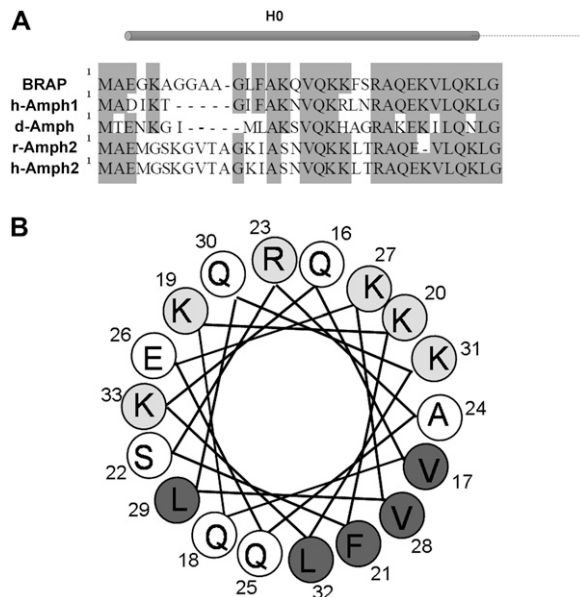


FIGURE 1 N-terminal amphipathic helix of the BAR domain of BRAP. (A) Alignments of N-terminal sequences (H0) of BRAP/Bin2 and several amphiphysins (Amph) show great degree of homology (h, human; d, *Drosophila*; r, rat). (B) Helical wheel representation of H0 from BRAP. Numbers indicate position of the amino acid. Hydrophobic residues are shaded.

dimerizes after incorporation in lipid membranes, providing a possible mechanism for generation of high-order oligomers of N-BAR domains. Monitoring the fluorescence of different membrane probes, our membrane insertion of H0-NBAR is shown to increase the packing of lipids both in the hydrophobic and headgroup regions of the bilayer. Finally, we also find that H0-NBAR is effective in inducing liposome fusion but has no liposome tubulation activity. Our results rule out the insertion of H0-NBAR in the exposed outer membrane leaflet as the mechanism of tubulation induced by N-BAR domains and point to a likely interplay between the membrane binding of H0-NBAR and the scaffold provided by the concave surface of the BAR domain.

## METHODS

### Materials

Peptides H0-NBAR, H0-NBAR-EDANS(5-((2-aminoethyl)amino)naphthalene-1-sulfonic acid), H0-NBAR-FITC(fluorescein isothiocyanate), and H0-ENTH(epsin N-terminal homology domain) were synthesized by Genemed Synthesis (San Francisco, CA). Labeling was achieved by conjugation on the N-terminal end of the peptide. The purity was always >95%.

1-Palmitoyl-2-oleoyl-*sn*-phosphocholine (POPC), 1-palmitoyl-2-oleoyl-*sn*-glycero-3-[phospho-*rac*-(1-glycerol)] (POPG), 1-palmitoyl-2-oleoyl-*sn*-glycero-3-(phospho-*l*-serine) (POPS), 1,2-dioleoyl-*sn*-glycero-3-phosphoethanolamine-*N*-(7-nitro-2-1,3-benzoxadiazol-4-yl) (NBD-DOPE), 1-oleoyl-2-[12-[(7-nitro-2-1,3-benzoxadiazol-4-yl)amino]dodecanoyl]-*sn*-glycero-phosphocholine (PC-NBD), 1-oleoyl-2-[12-[(7-nitro-2-1,3-benzoxadiazol-4-yl)amino]dodecanoyl]-*sn*-glycero-3-[phospho-*rac*-(1-glycerol)] (PG-NBD), 1-oleoyl-2-[12-[(7-nitro-2-1,3-benzoxadiazol-4-yl)amino]dodecanoyl]-*sn*-glycero-phosphoserine (PS-NBD), 1-oleoyl-2-[12-[(7-nitro-2-1,3-benzox-

adiazol-4-yl)amino]dodecanoyl]-*sn*-glycero-phosphate (PA-NBD), and 1,2-dioleoyl-*sn*-glycero-3-phosphoethanolamine-*N*-(lissamine rhodamine B sulfonyl) (Rho-DOPE) were from Avanti Polar Lipids (Alabaster, AL).

1,6-Diphenyl-1,3,5-hexatriene (DPH) and 5,6-carboxyfluorescein (5,6-CF) were from Molecular Probes (Eugene, OR). Brain extract from bovine brain (Folch fraction I) was from Sigma-Aldrich (St. Louis, MO).

Fine chemicals were obtained from Merck (Darmstadt, Germany). All materials were used without further purification.

### Liposome preparation

The desired amount of phospholipids was mixed in chloroform and dried under a  $N_{2(g)}$  flow. The sample was then kept in vacuum overnight. Liposomes were prepared with buffer Hepes 20 mM, NaCl 150 mM, pH 7.4. The hydration step was performed with gentle addition of buffer followed by freeze-thaw cycles. Large unilamellar vesicles (LUV) were produced by extrusion through polycarbonate filters (12) in an Avestin (Ottawa, Ontario, Canada) extruder. Liposomes with 5,6-CF encapsulated were prepared by hydration with buffer Hepes 20 mM, NaCl 150 mM, pH 8.4 with 5 mM 5,6-CF. After extrusion, the suspension was passed through a 10 ml Econo-Pac 10DG column Bio-Gel P-6DG gel from Bio-Rad (Hercules, CA) with 6 kDa molecular mass exclusion) and eluted with buffer Hepes 20 mM, NaCl 150 mM, pH 8.4.

### Circular dichroism spectroscopy

Circular dichroism (CD) spectroscopy was performed on a Jasco J-720 spectropolarimeter with a 450 W Xe lamp. Lipid suspensions were extruded using polycarbonate filters of 0.1  $\mu$ m. Peptide concentration was 40  $\mu$ M.

### Fluorescence spectroscopy

Steady-state fluorescence measurements were carried out with an SLM 8100 Series 2 spectrofluorimeter (SLM-Aminco, Spectronics, Rochester, NY) described in detail elsewhere (13).

Fluorescence anisotropies were determined as described in Lakowicz (14). Time-resolved fluorescence measurements of H0-BAR-EDANS were carried out with a time-correlated single-photon timing system, which is also described elsewhere (13). For steady-state fluorescence anisotropies and time-resolved fluorescence measurements with H0-NBAR-EDANS, the excitation and emission wavelengths were 340 nm and 460 nm, respectively. For time-resolved fluorescence measurements with H0-NBAR-FITC, the excitation and emission wavelengths were 470 nm and 525 nm, respectively. Analysis of fluorescence intensity and anisotropy decays was carried out as previously described (15,16). All measurements were performed at room temperature.

### Cryoelectron microscopy

Samples were applied to holey-carbon grids Quantifoil 2/2 (Jena, Germany) and plunged into liquid ethane in a Leica EM-CPC (Wetzlar, Germany). Images were recorded under low dose conditions by a Gatan slow-scan charge-coupled device (model 694) on a FEI TecnaiG<sup>2</sup> electron cryomicroscope (Hillsboro, OR) operating at 200 KV at different magnifications.

## RESULTS

### The N-terminal segment of the N-BAR domain is 100% $\alpha$ -helical in anionic liposomes

CD measurements were performed on the unlabeled H0-NBAR peptide while in the absence of liposomes and in the presence of zwitterionic liposomes (POPC) and anionic liposomes (POPG) (Fig. 2). CD measurements of the labeled

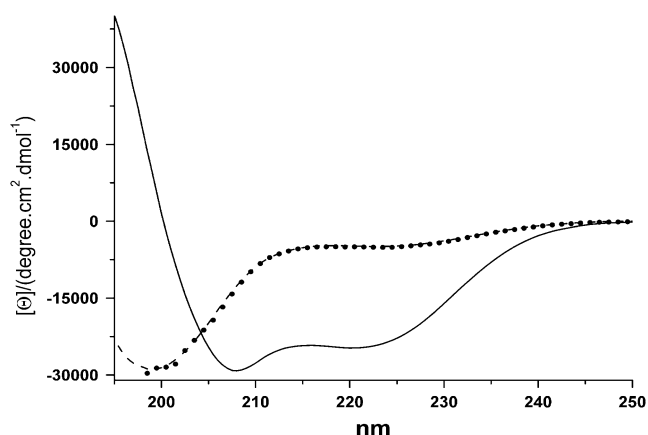


FIGURE 2 N-terminal sequence of the BAR domain is  $\alpha$ -helical in anionic liposomes. CD spectrum of H0 in buffer (dashed curve) and in the presence of POPC (●) and POPG liposomes (solid curve). Lipid concentration was 1 mM.

H0-NBAR peptides (both H0-NBAR-EDANS and H0-NBAR-FITC) produced the same results, confirming that labeling did not change the structure of H0-NBAR (results not shown). Deconvolution of the obtained spectrum with the CDNN CD Spectra Deconvolution v. 2.1 software revealed a predominantly unstructured peptide in the absence of lipids and in the presence of 1 mM of POPC. After addition of 1 mM of POPG, the peptide presented  $>80\%$   $\alpha$ -helical structure, compatible with the expected amphipathic nature of the N-terminal segment of the N-BAR domain while interacting with lipid membranes.

### Interaction of H0-NBAR with lipid bilayers is only dependent on lipid charge

The fluorescence emission spectrum from H0-NBAR-EDANS is practically unaffected upon interaction with lipid bilayers, as the wavelength of maximum emission intensity remains the same and only a small broadening in the lower wavelength range of the spectrum is visible (results not shown). EDANS emission spectrum is extremely sensitive to the environment (17) and this result is an indication that the EDANS fluorophore is located in the hydrophilic face of the amphipathic helix and that it remains fully exposed to the aqueous environment. There was, however, a subtle difference in quantum yields (20% higher in the presence of anionic phospholipids) and a significant change in fluorescence anisotropy, from  $\langle r \rangle = 0.022$  in buffer to  $\langle r \rangle = 0.06$  in the presence of anionic phospholipids. This change in fluorescence anisotropy is the result of the immobilization of the peptide in the lipid bilayer and can be used to quantify the partition of H0-NBAR to bilayers from Eq. 1 (18),

$$\langle r \rangle = \frac{\langle r \rangle_w + K_p \times \gamma_L \times [L] \times \langle r \rangle_L}{1 + K_p \times \gamma_L \times [L]}, \quad (1)$$

where  $\langle r \rangle_w$  is the fluorescence anisotropy in water,  $\langle r \rangle_L$  is the fluorescence anisotropy in the bilayer,  $\gamma_L$  is the molar volume of the lipid,  $[L]$  is the lipid concentration, and  $K_p$  is the lipid/water partition coefficient.

Fig. 3 A shows the dependence of  $\langle r \rangle$  on the lipid concentration for different phospholipids. It is clear that partition to POPC liposomes is extremely low when compared to the partition observed for both anionic phospholipids POPS and POPG.

The results of fitting Eq. 1 to the data in Fig. 3 are presented in Table 1. Partition of H0-NBAR to POPS and POPG liposomes

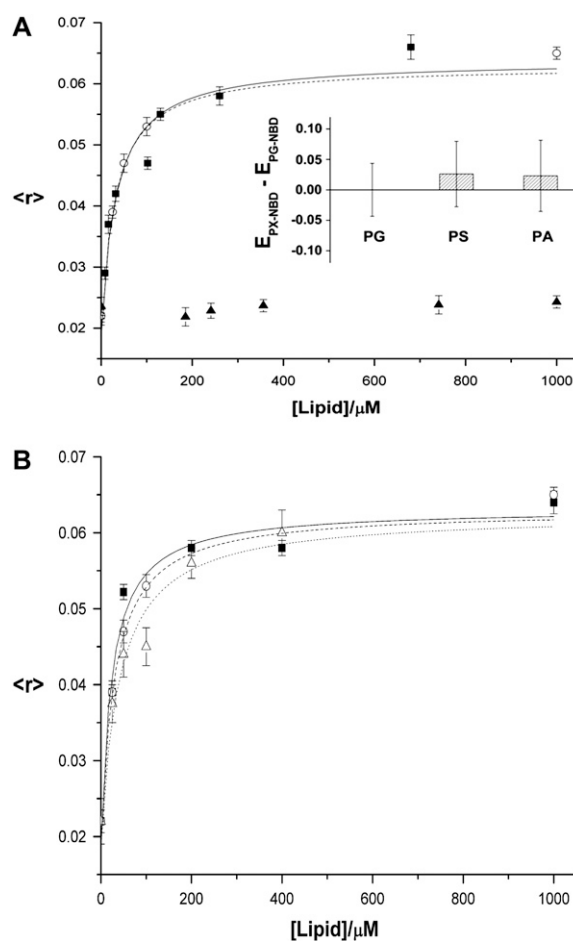


FIGURE 3 Partition of H0 to bilayers is only sensitive to charge. (A) Increase of fluorescence emission anisotropy of H0-EDANS with lipid concentration. H0-EDANS in the presence of POPC (▲), POPG (○), and POPS (■) liposomes of 100 nm diameter. (Inset) Efficiencies of energy transfer from H0-NBAR-EDANS to NBD-labeled phospholipids (PX-NBD) in POPG liposomes. Bars show the difference in FRET efficiency ( $E$ ) relative to the value obtained for PG-NBD ( $E_{PG-NBD} = 0.38$ ). Concentration of PX-NBD in POPG bilayers was 2% (mol/mol). (B) Increase of fluorescence emission anisotropy of H0-EDANS with POPG concentration for different liposome sizes. H0-EDANS in the presence of POPG liposomes with 30 (Δ), 100 (○), and 400 (■) nm radius. Fluorescence emission anisotropies were measured with excitation wavelength of 340 nm and emission wavelength of 460 nm. In both panels, the lines are the fits of Eq. 1 to the data, as described in the text.

**TABLE 1** Membrane/water partition coefficients ( $K_p$ ) for H0-NBAR-EDANS determined from fluorescence anisotropies (Fig. 3)

Vesicles	$K_p$
POPC*	$(5.6 \pm 2.7) \times 10^1$
POPS	$(4.2 \pm 1.0) \times 10^4$
POPG (diameter 30 nm)	$(3.2 \pm 1.1) \times 10^4$
POPG (diameter 100 nm)	$(4.4 \pm 0.9) \times 10^4$
POPG (diameter 400 nm)	$(5.5 \pm 1.5) \times 10^4$

\*This  $K_p$  value is a lower bound assuming that the anisotropy of the peptide population in interaction with POPC is identical as the one obtained with anionic phospholipids ( $\langle r \rangle \sim 0.06$ ).

somes is identical, suggesting that the nature of the anionic phospholipid is irrelevant for H0-NBAR interaction with liposomes. Further evidence for the absence of a specific interaction with a class of lipids can be obtained from a FRET assay, where lipids (e.g. PS, PA, and PG) are derivatized with an acceptor (NBD) for FRET from EDANS, and dispersed (2% mol/mol concentration) in a POPG matrix.

FRET efficiencies ( $E$ ) are obtained from the extent of fluorescence emission quenching of the donor induced by the presence of acceptors,

$$E = 1 - \frac{I_{DA}}{I_D} = 1 - \frac{\int_0^\infty i_{DA}(t)}{\int_0^\infty i_D(t)}, \quad (2)$$

where  $I_{DA}$  and  $I_D$  are the steady-state fluorescence intensities of the donor in the presence and absence of acceptors, respectively, and  $i_{DA}(t)$  and  $i_D(t)$  are the donor fluorescence decays in the presence and absence of acceptors, respectively.

In case there was a specific interaction between H0-NBAR-EDANS and the NBD-labeled phospholipid, the peptide would be incorporated in the vicinity of that lipid and FRET would increase. Since there is also liposome fusion induced by H0-NBAR-EDANS (see later), the available two-dimensional FRET formalisms may not be applicable for retrieving quantitative information about H0-NBAR-EDANS selectivity for a specific phospholipid (19), and a more qualitative approach was used. The results are shown in the inset of Fig. 3 A. It is clear that no significant differences exist among the  $E$  obtained with any of the anionic phospholipids. The small differences in FRET efficiencies are a result of the lack of selectivity of H0-NBAR-EDANS for specific phospholipids.

Partition of H0-NBAR-EDANS to lipid membranes is also insensitive to the dimensions of the liposomes and hence insensitive to the degree of curvature of the bilayer in this range of liposome size (Fig. 3 B). Even though the values of  $K_p$  recovered for larger liposomes are slightly higher (as seen in Table 1), the differences are within the errors of the fits and thus nonsignificant.

Residual partition to POPC liposomes was detected. After long incubation times (overnight), an increase of fusion of POPC liposomes loaded with H0-NBAR was evident relative

to blank POPC vesicles. This was clear from a FRET experiment carried out with a mixture of liposomes loaded with 2% NBD-DOPE (donor) and liposomes loaded with 2% Rho-DOPE (acceptor). The increase of FRET efficiencies after the mixture reports fusion of the liposomes. H0-NBAR stimulated fusion for both POPG (considerably) and POPC liposomes (slightly) (Fig. 4) and was more effective in doing so than a control peptide (H0-ENTH), corresponding to the helix 0 of the epsin N-terminal homology domain that is also related to membrane curvature induction (albeit in the case of epsin the presence of phosphatidylinositol-(4,5)-bisphosphate PIP(4,5)<sub>2</sub> is required for membrane remodeling) (20). It was checked that under these conditions H0-ENTH is completely bound to liposomes (results not shown).

### H0-NBAR is an antiparallel dimer in the membrane

The function of H0-NBAR in liposome tubulation mediated by the BAR domain was recently proposed to be related to BAR domain oligomerization (7).

With the intent to verify if H0-NBAR oligomerizes in the membrane, FRET measurements were performed using H0-NBAR-EDANS as a donor and H0-NBAR-FITC as an acceptor (emission and absorption spectra are in the Supplementary Material).

For this system, the high Förster radius ( $R_0$ ) of the EDANS-FITC donor-acceptor pair ( $R_0$  (EDANS-FITC) = 40 Å) entails a small contribution of energy transfer between nonoligomerized H0-NBAR, and this was taken into account in our analysis (see FRET simulation for the monomeric

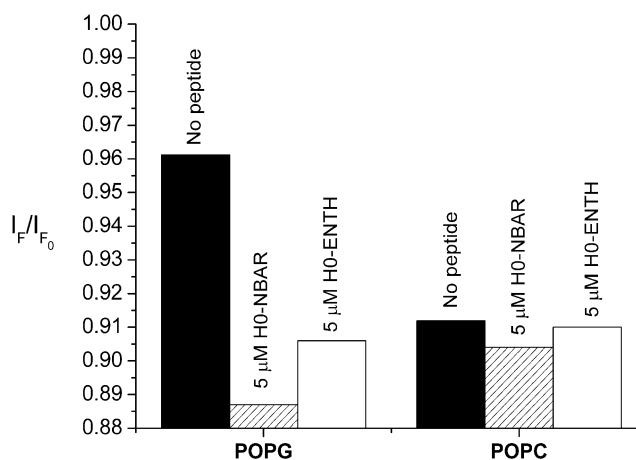


**FIGURE 4** H0-NBAR promotes liposome fusion in both POPC and POPG. Decrease in fluorescence emission intensities of NBD-DOPE 15 min after mixing of liposomes with 2% NBD-DOPE and liposomes with 2% Rho-DOPE in the presence and in the absence of H0-NBAR. Results obtained with H0-ENTH are shown for comparison. Fluorescence intensity in the absence of acceptor was measured and no significant donor fluorescence bleaching was detected. Fluorescence intensities were obtained with excitation and emission wavelengths set to 460 and 510 nm, respectively.

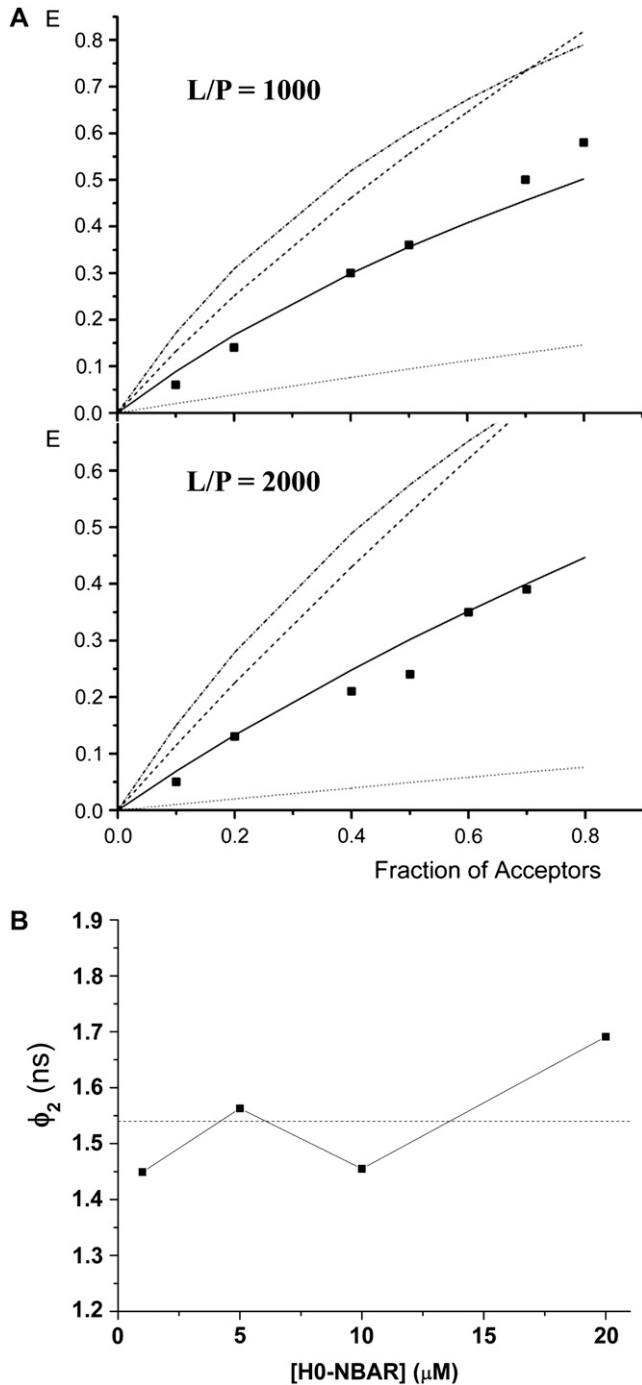


FIGURE 5 H0 forms an antiparallel dimer in POPG bilayers. (A) FRET efficiencies determined from the integration of H0-EDANS fluorescence decays in the presence of increasing fraction of acceptors (H0-FITC) (■) at a L/P = 1000 and 2000. Simulations for FRET between monomers (dotted line), parallel dimers (dashed line) or trimers (dash-dotted line) do not describe the data accurately. The simulation which provided a more accurate description of the data was obtained for an antiparallel dimer (solid line) in which EDANS and FITC are separated by 43 Å (the estimated size of H0-NBAR is 49.5 Å). Insensitivity to L/P ratios further supports the derived formalisms. (B) Dependence of the longer rotational correlation time ( $\phi_2$ ) of the fluorescence anisotropy decay of H0-NBAR-FITC on the concentration of peptide in buffer. The dotted line is the expected  $\phi_2$  for a H0-NBAR monomer. The dynamics of H0-NBAR-FITC is virtually unaffected by the

hypothesis in Fig. 5 A). The donor fluorescence decay in the presence of acceptors is described as

$$i_{DA}(t) = \left[ \sum_{k=1}^{n-1} f_{Dq}(k) \times \rho_{\text{bound}}^{n-k}(t) \right] \times i_D(t) \times \rho_{\text{nonbound}}(t) + \left( 1 - \sum_{k=1}^{n-1} f_{Dq}(k) \right) \times i_D(t) \times \rho_{\text{nonbound}}(t), \quad (3)$$

where  $\rho_{\text{bound}}$  is the FRET contribution from energy transfer to each acceptor in the oligomer containing the donor,  $\rho_{\text{nonbound}}$  is the FRET contribution arising from energy transfer to acceptors that are not integrated in the same oligomer as the donor, and  $f_{Dq}(k)$  is the fraction of donors bound to  $k$  acceptors

$$f_{Dq}(k) = k \times \binom{n}{k} \times P_D^k P_A^{n-k}. \quad (4)$$

Here  $n$  is the number of units in the oligomer,  $k$  counts the number of donors,  $P_D$  is the mole ratio of donors, and  $P_A$  is the mole ratio of acceptors.

Through measurement of the dependence of FRET efficiencies on the acceptor/donor ratio, it is possible to conclude about the presence of oligomerization and to gather information on the type of oligomerization found (21). The contribution for FRET from each acceptor in the same oligomer as the donor is given by

$$\rho_{\text{bound}} = \exp\left(-\frac{1}{\tau_0} \times \left(\frac{R_0}{r_{D-A}}\right)^6\right), \quad (5)$$

where  $\tau_0$  is the lifetime of the donor in the absence of acceptors, and  $r_{D-A}$  is the distance between the donor and the acceptor inside the oligomer.

Equation 6 gives  $\rho_{\text{nonbound}}$  for a two-dimensional system (15):

$$\rho_{\text{nonbound}} = \exp\left[-n_2 \times \pi \times \Gamma(2/3) \times R_0^2 \times \left(\frac{t}{\tau_0}\right)^{\frac{1}{3}}\right], \quad (6)$$

where  $n_2$  is the acceptor density in each bilayer leaflet, and  $\Gamma$  is the  $\gamma$ -function.

From Eqs. 2–6, simulations for FRET efficiencies are obtained (Fig. 5 A). In the FRET analysis, the different oligomerization models were fitted to two series of data simultaneously. In the first series, the lipid/protein ratio (L/P) equals 1000 whereas in the second the protein was diluted twofold (L/P = 2000). With this methodology, uncertainty resulting from erroneous quantification of the two FRET contributions (to acceptors within the same oligomers and to unbound acceptors) is eliminated. The oligomerization

increase in concentration and the recovered longer correlation time is in agreement with the rotation of a H0 monomer (see text). All samples contained the same concentration of H0-NBAR-FITC, and different concentrations of H0-NBAR were obtained through addition of unlabeled peptide.

model that provided the best fit to the two data series was one that considered dimerization of the peptide and a distance of 43 Å between donor and acceptor inside the dimer. This distance is in good agreement with an antiparallel dimer as the size of a rigid and fully  $\alpha$ -helical H0-NBAR is expected to be  $\sim 49.5$  Å (1.5 Å per residue). The sensitivity of the methodology chosen is clear from the comparison with the simulations for FRET efficiencies arising from a parallel dimer ( $r_{D-A} < 20$  Å) and other oligomerization numbers (see Fig. 5 A).

The oligomerization of H0-NBAR is dependent on membrane binding, as the peptide exists as a monomer while in buffer. This was concluded from anisotropy decays of H0-NBAR-FITC (Supplementary Material). The anisotropy decays were well described by two rotational correlation times,  $\phi_1$  and  $\phi_2$ :

$$r(t) = r_0 \times \left[ \beta_1 \times \exp\left(\frac{-t}{\phi_1}\right) + \beta_2 \times \exp\left(\frac{-t}{\phi_2}\right) \right]. \quad (7)$$

Here  $r_0$  is the fundamental anisotropy, and  $\beta_1$  and  $\beta_2$  are the component amplitudes. The methodology for analysis of time-resolved anisotropy decays is described in detail elsewhere (16).

$\phi_1$  was typically smaller than 250 ps and is expected to be related to independent and fast movement of the FITC fluorophore. The recovered  $\phi_2$  values were between 1.45 and 1.69 ns (Fig. 5 B) and are expected to correspond to the motion of the entire peptide. The rotational correlation time can be estimated from the following equation (strictly valid for spherical molecules):

$$\phi = \frac{\eta \times V}{R \times T}, \quad (8)$$

where  $\eta$  is the viscosity of the medium,  $V$  is the molar volume of the molecule,  $R$  is the ideal gas constant, and  $T$  is the temperature. From Eq. 8 and taking into consideration the hydration volume for a protein (22) the expected  $\phi_2$  of monomeric H0-NBAR is 1.54 ns (Fig. 5 B). Hence, H0-NBAR dynamics in solution is as expected for a monomer and is independent of concentration up to 20  $\mu$ M of peptide.

### H0-NBAR does not translocate efficiently across the bilayer

When bound to the full N-BAR domain, H0-NBAR is expected to interact with only one monolayer. The structural changes induced in the exposed monolayer and the resulting monolayer asymmetry could be responsible for membrane bending mediated by N-BAR, in a similar mechanism as the one observed for the ENTH domain of epsin after PIP(4,5)<sub>2</sub> binding (23). To study if the H0-NBAR is able to induce by itself the sort of membrane bending observed with full N-BAR domains, it is necessary to determine if the peptide, after interaction with anionic liposomes, remains bound to

the outer monolayer, or if it exhibits fast translocation across the bilayer. If H0-NBAR translocated efficiently across the bilayer, effects on both monolayers would limit monolayer asymmetry, and consequently H0-NBAR would not behave in a comparable manner as the helix 0 in the N-terminal segment of N-BAR.

To evaluate this, the following methodology was applied. The iodide ion exhibits low permeability across lipid bilayers (Fig. 6, *inset*), and by measuring the degree of fluorescence quenching induced by  $I^-$  on H0-NBAR-EDANS, it is possible to estimate the fraction of H0-NBAR-EDANS that translocated across the bilayer. Two sets of samples were measured. In the first, 1 mM POPG liposomes were incubated with 2  $\mu$ M of H0-NBAR-EDANS for only 3 min, as this amount of time guarantees almost complete binding of the peptide to the membrane (results not shown). In the second set of samples, the same concentrations of POPG liposomes and H0-NBAR-EDANS were incubated for 40 min. The fluorescence intensities were measured immediately before and after addition of KI and the Stern-Volmer plots for fluorescence quenching were obtained (Fig. 6). It is clear that the difference between the degree of exposure of H0-NBAR to KI is minimal between the two data sets. Assuming that H0-NBAR-EDANS in the inside of vesicles was 100% inaccessible to KI, after 40 min of incubation, there was only a maximum of 4% translocated H0-NBAR.

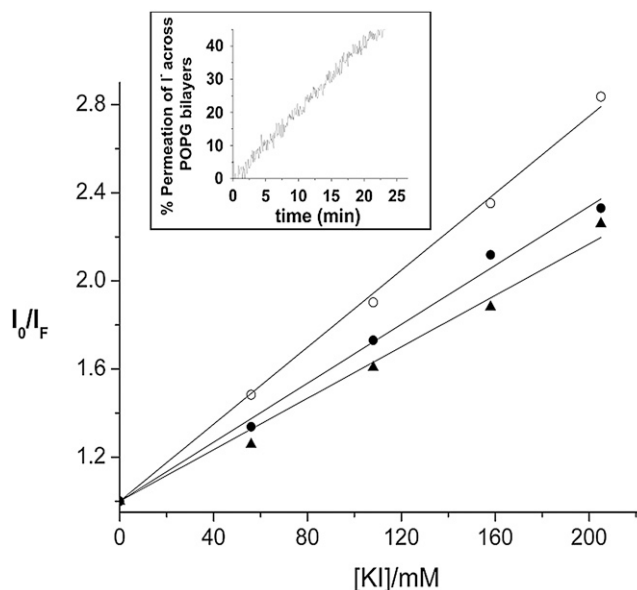
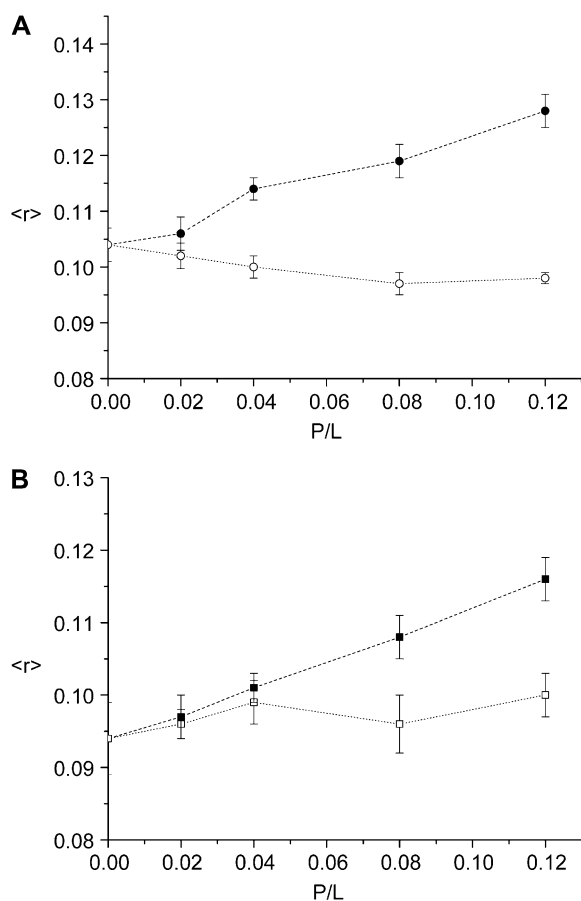


FIGURE 6 Translocation of H0-NBAR in POPG liposomes is very slow. Stern-Volmer plots for fluorescence emission quenching of H0-NBAR-EDANS by iodide. H0-EDANS in buffer (○) and in the presence of POPG liposomes with a 3 min (●) and 40 min (▲) incubation time before addition of iodide quencher. Permeation of iodide across the bilayer is slow (see *inset*), and after 40 min the amount of H0-NBAR-EDANS that translocated through the bilayer is estimated to be a maximum of 4%. (*Inset*) Permeation of  $I^-$  across POPG liposomes as measured by fluorescence quenching of encapsulated 5,6-CF.

### H0-NBAR increases packing of anionic phospholipids at a higher degree than a control peptide

The effect of unlabeled H0-NBAR in the packing and dynamics of phospholipids was measured through the fluorescence anisotropy of two lipid membrane probes, NBD-DOPE and DPH. The first is a good probe for the headgroup region of the bilayer whereas the second is a well-known probe of acyl chain packing. The effects of adding increasing amounts of H0-NBAR to POPG liposomes loaded with 1% (mol/mol) of fluorescent probe are shown in Fig. 7. The results obtained with H0-ENTH are also shown for comparison. ENTH is thought to be able to tubulate liposomes in the presence of PIP(4,5)<sub>2</sub> through insertion of H0-ENTH in the acyl chain. In the absence of this lipid, H0-ENTH is unable to penetrate the membrane (6). It should be stressed that the induced probe



**FIGURE 7** H0-NBAR increases phospholipid packing. (A) Effect of unlabeled H0-NBAR on the fluorescence emission anisotropy of NBD-DOPE (●). NBD-DOPE fluorescence is sensitive to changes in the headgroup region of the bilayer. (B) Effect of unlabeled H0-NBAR on the fluorescence emission anisotropy of DPH (■). DPH fluorescence is sensitive to changes in the acyl-chain region of the bilayer. For comparison, the effect on both probes of an amphipathic peptide, which is not expected to insert in the bilayer (H0-ENTH), is also presented (open symbols). Lines serve as guides to the eye.

anisotropy increase is not related to a decrease of its lifetime (Perrin equation (14)), since the probe fluorescence intensity is invariant (there is no fluorescence quenching) upon peptide addition (results not shown).

H0-NBAR clearly rigidifies both the acyl chains and the headgroup region of the bilayer. H0-ENTH has only minor effects on the fluorescence anisotropy of both probes even at very high concentrations, confirming that H0-NBAR is particularly rigidifying for phospholipid packing.

### H0-NBAR is not able to tubulate lipid membranes in the absence of the scaffold domain of N-BAR

Cryoelectron microscopy was used to monitor the effects of H0-NBAR on liposome morphology (Fig. 8). H0-NBAR is clearly not able to induce tubulation of liposomes composed of pure synthetic phospholipids (POPG) (Fig. 8) or of lipid brain extracts (results not shown). The only noticeable effect of H0-NBAR was the fusion of the liposomes (results not shown) and a 5–20 Å increase in average membrane thickness, without a significant change in their morphology or size. Different P/L ratios produced similar results.

## DISCUSSION

Proteins are believed to be able to induce membrane bending by means of three mechanisms, namely the scaffold, local spontaneous curvature, and the bilayer-couple mechanism (24). In the scaffold mechanism, proteins force their intrinsic curvature to the lipid membrane. This intrinsic curvature can be the result of tertiary structure or of the surface from a protein network. In the local spontaneous curvature hypothesis, a shallow insertion in the lipid membrane of an amphipathic moiety from a protein induces local perturbation of the packing of lipid headgroups resulting in local deformation of the bilayer. Finally, in the bilayer-couple mechanism, the insertion of an amphipathic helix in the lipid bilayer could result in an increase of the area of the monolayer where the protein is inserted that is compensated by an increase of bilayer curvature.

The presence of H0-NBAR greatly enhances the liposome tubulation activity of BAR domains. Several theories have been recently presented to explain the relevance of H0-NBAR in this phenomenon. It is feasible that the sole function of H0-NBAR is the increase in residence time of the BAR domain in the membrane by tight binding to the hydrophobic interior of the bilayer, but it is also possible that this segment is important in the oligomerization of BAR domains in the membrane, since cross-linking experiments suggest that BAR domains exist in membranes as high-order oligomers (5,25).

Therefore, N-BAR domains could induce remodeling of membranes by the scaffold, the local spontaneous curvature and the bilayer-couple mechanisms, or by a combination of those. The concave shape of the BAR dimer can act as a

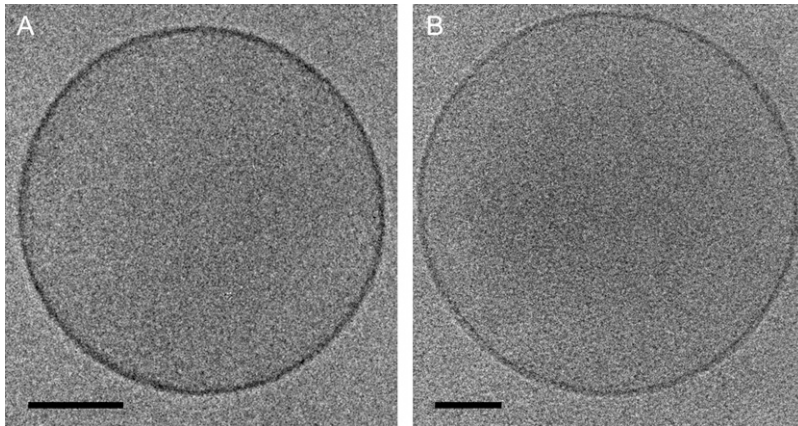


**FIGURE 8** H0-NBAR does not alter liposome morphology. (A) Electron micrographs from POPG liposomes. (B) Electron micrographs from POPG liposomes after incubation with H0-NBAR (L/P = 10). Although the size is not completely regular in the sample with or without the peptide incubation, the spherical morphology is identical in both cases. In both cases, the scale bar represents 50 nm.

scaffold, forcing the membrane curvature to adapt to its own curvature. Insertion of the amphipathic helix could also act through either the bilayer-couple or the local spontaneous curvature mechanism.

Here we showed that insertion of H0-NBAR in the lipid bilayer is unable to induce significant changes in lipid membrane morphology. Recently, some authors reported that highly amphipathic peptides induced liposomes or supported lipid bilayers to adopt tubular structures when present at very high concentrations (L/P < 10) (26,27). However, these concentrations are virtually biologically unfeasible, as for the protein-exposed monolayer they correspond to a maximum L/P of 5. For the BAR domain-containing proteins, this would mean docking one protein to the membrane for each five phospholipids of the exposed monolayer, which is impossible considering the dimensions of the BAR domain alone. Hence, another mechanism must be responsible for the enhanced membrane bending activity of the BAR domain in the presence of H0-NBAR.

The main contribution for H0-NBAR binding to liposomes is shown here to be electrostatic. This is at variance with the proposal that H0-NBAR's function is to stabilize the bound conformation of the BAR domain through strong hydrophobic interactions with the membrane. Although partition of H0-NBAR to anionic liposomes is very efficient, it is unlikely to be higher than the partition of the BAR domain itself, as the concave surface of the BAR domain dimer is already strongly positively charged. Partition of H0-NBAR to anionic bilayers disturbs both the headgroup as the acyl-chain regions of the bilayer. H0-NBAR is more disturbing to the bilayer than H0-ENTH, and this can be the result of H0-NBAR dimerization in the membrane environment, as dimerization of amphipathic peptides was previously shown to be particularly disturbing to bilayer structure (28).

The oligomerization of the H0-NBAR peptide explains the detection of high-order oligomers of N-BAR domains (5,25) as it would allow for efficient association of several BAR domain dimers, and if effective in the full BAR domain, can be the mechanism by which H0-NBAR provides a more

favorable framework for tubulation mediated by N-BAR (7). The antiparallel orientation of such associations could allow for the formation of highly aligned high-order oligomers of BAR domains in the membrane environment as previously suggested (5).

A recent molecular dynamics study (29) showed binding of N-BAR domains to a lipid membrane resulting in generation of membrane curvature through the scaffold mechanism. Results suggested that the main role of the N-terminal amphipathic helix of N-BAR was to favor the orientation of the N-BAR domain that allowed direct interaction between the membrane and the protein concave face. In effect, from our result, it is clear that the membrane-bending activity of the N-BAR domain must be achieved through the scaffold mechanism in which the BAR domain presents its concave surface to the membrane, and forces the membrane to adopt the same curvature, whereas H0-NBAR only plays a promoting role in this process, either by: i), enhancing the membrane affinity of the full N-BAR domain; ii), mediating N-BAR high-order oligomerization and stimulating the increase of local concentrations of the protein; iii), increasing lipid packing and facilitating curvature generation; or iv), forcing the protein to present its concave face to the membrane or by a combination of these mechanisms.

## SUPPLEMENTARY MATERIAL

To view all of the supplemental files associated with this article, visit [www.biophysj.org](http://www.biophysj.org).

F. F. acknowledges grant SFRH/BD/14282/2003 from Fundação para a Ciência e a Tecnologia (FCT) (Portugal). A.F. acknowledges grant SFRH/BPD/26150/2005 from FCT (Portugal). This work was funded by FCT (Portugal) under the program POCI.

## REFERENCES

1. Farsad, K., and P. De Camilli. 2003. Mechanisms of membrane deformation. *Curr. Opin. Cell Biol.* 15:372–381.

2. McMahon, H. T., and J. L. Gallop. 2005. Membrane curvature and mechanisms of dynamic cell membrane remodeling. *Nature*. 438: 590–596.
3. Takei, K., V. Haucke, V. Slepnev, K. Farsad, M. Salazar, H. Chen, and P. De Camilli. 1998. Generation of coated intermediates of clathrin-mediated endocytosis on protein-free liposomes. *Cell*. 94:131–141.
4. Takei, K., V. I. Slepnev, V. Haucke, and P. De Camilli. 1999. Functional partnership between amphiphysin and dynamin in clathrin-mediated endocytosis. *Nat. Cell Biol.* 1:33–39.
5. Farsad, K., N. Ringstad, K. Takei, S. R. Floyd, K. Rose, and P. De Camilli. 2001. Generation of high curvature membranes mediated by direct endophilin bilayer interactions. *J. Cell Biol.* 155:193–200.
6. Ford, M. G. J., I. G. Mills, B. J. Peter, Y. Vallis, G. J. K. Praefcke, P. R. Evans, and H. T. McMahon. 2002. Curvature of clathrin-coated pits driven by epsin. *Nature*. 419:361–366.
7. Gallop, J. L., and H. T. McMahon. 2005. BAR domains and membrane curvature: bringing your curves to the BAR. *Biochem. Soc. Symp.* 72: 223–231.
8. Peter, B. J., H. M. Kent, I. G. Mills, Y. Vallis, P. J. G. Butler, P. R. Evans, and H. T. McMahon. 2004. BAR domains as sensors of membrane curvature: the amphiphysin BAR structure. *Science*. 303:495–499.
9. Gallop, J. L., C. C. Jao, H. M. Kent, P. J. G. Butler, P. R. Evans, R. Langen, and H. T. McMahon. 2006. Mechanism of endophilin N-BAR domain-mediated membrane curvature. *EMBO J.* 25:2898–2910.
10. Ge, K., and G. C. Prendergast. 2000. Bin2, a functionally nonredundant member of the BAR adaptor gene family. *Genomics*. 67:210–220.
11. Greiner, J., M. Ringhoffer, M. Taniguchi, T. Hauser, A. Schmitt, H. Döhner, and M. Schmitt. 2003. Characterization of several leukemia-associated antigens inducing humoral immune responses in acute and chronic myeloid leukemia. *Int. J. Cancer*. 106:224–231.
12. Mayer, L. D., M. J. Hope, and P. R. Cullis. 1986. Vesicles of variable sizes produced by a rapid extrusion procedure. *Biochim. Biophys. Acta*. 858:161–168.
13. Loura, L. M. S., A. Fedorov, and M. Prieto. 2001. Fluid-fluid membrane microheterogeneity: a fluorescence resonance energy transfer study. *Biophys. J.* 80:776–788.
14. Lakowicz, J. R. 1999. Principles of Fluorescence Spectroscopy. Kluwer Academic/Plenum Publishers, New York.
15. Loura, L. M. S., A. Fedorov, and M. Prieto. 1996. Resonance energy transfer in a model system of membranes: application to gel and liquid crystalline phases. *Biophys. J.* 71:1823–1836.
16. de Almeida, R. F. M., L. S. M. Loura, M. Prieto, A. Watts, A. Fedorov, and F. J. Barrantes. 2006. Structure and dynamics of the  $\gamma$ -M4 transmembrane domain of the acetylcholine receptor in lipid bilayers: insights into receptor assembly and function. *Mol. Membr. Biol.* 23: 305–315.
17. Hudson, E. N., and G. Weber. 1973. Synthesis and characterization of two fluorescent sulfhydryl reagents. *Biochemistry*. 12:4154–4161.
18. Santos, N. C., M. Prieto, and M. A. R. B. Castanho. 2003. Quantifying molecular partition into model systems of biomembranes: an emphasis on optical spectroscopic methods. *Biochim. Biophys. Acta*. 1612: 123–135.
19. Fernandes, F., L. M. S. Loura, R. Koehorst, R. B. Spruijt, M. A. Hemminga, A. Fedorov, and M. Prieto. 2004. Quantification of protein-lipid selectivity using FRET: application to the M13 major coat protein. *Biophys. J.* 87:344–352.
20. Itoh, T., K. Koshiba, T. Kigawa, A. Kikuchi, S. Yokoyama, and T. Takenawa. 2001. Role of the ENTH domain in phosphatidylinositol-4,5-bisphosphate binding and endocytosis. *Science*. 291:1047–1051.
21. Adair, B. D., and D. M. Engelman. 1994. Glycophorin A helical transmembrane domains dimerize in phospholipid bilayers: a resonance energy transfer study. *Biochemistry*. 33:5539–5544.
22. Durchschlag, H., and P. Zipper. 2001. Comparative investigations of biopolymer hydration by physicochemical and modeling techniques. *Biophys. Chem.* 93:141–157.
23. Stahelin, R. V., F. Long, B. J. Peter, D. Murray, P. De Camilli, H. T. McMahon, and W. Cho. 2003. Contrasting membrane interaction mechanisms of AP180 N-terminal homology (ANTH) and epsin N-terminal homology (ENTH) domains. *J. Biol. Chem.* 278:28993–28999.
24. Zimmerberg, J., and M. M. Kozlov. 2006. How proteins produce cellular membrane curvature. *Nat. Rev. Mol. Cell Biol.* 7:9–19.
25. Richnau, N., A. Fransson, K. Farsad, and P. Aspenstrom. 2004. RICH-1 has a BIN/Amphiphysin/Rvsp domain responsible for binding to membrane lipids and tubulation of liposomes. *Biochem. Biophys. Res. Commun.* 320:1034–1042.
26. Furuya, T., T. Kiyota, S. Lee, T. Inoue, G. Sugihara, A. Logvinova, P. Goldsmith, and H. M. Ellerby. 2003. Nanotubes formed by highly hydrophobic amphiphilic  $\alpha$ -helical peptides and natural phospholipids. *Biophys. J.* 84:1950–1959.
27. Domanov, Y. A., and P. K. J. Kinnunen. 2006. Antimicrobial peptides temporins B and L induce formation of tubular lipid protrusions from supported phospholipid bilayers. *Biophys. J.* 91:4427–4439.
28. Hristova, K., C. E. Dempsey, and S. H. White. 2001. Structure, location, and lipid perturbations of melittin at the membrane interface. *Biophys. J.* 80:801–811.
29. Blood, P. D., and G. A. Voth. 2006. Direct observation of Bin/amphiphysin/Rvs (BAR) domain-induced membrane curvature by means of molecular dynamics simulations. *Proc. Natl. Acad. Sci. USA*. 103:15068–15072.